On the microstructure and mechanical property of as-extruded Mg-Gd-Y-Zn alloy with Sr addition

Shengming Liu, Hui Diao, Linjiang Chai, Bo Song

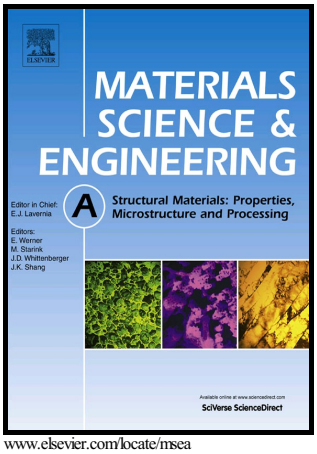

www.elsevier.com/locate/msea

PII: S0921-5093(16)31224-2
DOI: http://dx.doi.org/10.1016/j.msea.2016.10.016
Reference: MSA34218

To appear in: *Materials Science & Engineering A*

Received date: 8 September 2016
Revised date: 1 October 2016
Accepted date: 4 October 2016

Cite this article as: Shengming Liu, Hui Diao, Linjiang Chai and Bo Song, O the microstructure and mechanical property of as-extruded Mg-Gd-Y-Zn alloy with Sr addition, *Materials Science & Engineering A* http://dx.doi.org/10.1016/j.msea.2016.10.016

On the microstructure and mechanical property of as-extruded Mg-Gd-Y-Zn alloy with Sr addition

Shengming Liu [a], Hui Diao [b], Linjiang Chai [c], Bo Song [d,*]

[a] College of Materials Science and Engineering, Xihua University, Chengdu 610039, China

[b] Centre for Microscopy & Microanalysis, Faculty of Science, University of Queensland, Brisbane 4072, Australia

[c] College of Materials Science and Engineering, Chongqing University of Technology, Chongqing 400054, China

[d] Faculty of Materials and Energy, Southwest University, Chongqing 400715, China

[*]Corresponding author. Postal address: Tian Sheng Road 2#, Bei Bei District, Chongqing, China.

bosong@swu.edu.cn

Abstract

In this study, microstructure evolutions of Mg-6Gd-3Y-0.1Zn-xSr (x=0, 0.2, 0.6) alloys (named as sample 0Sr, 0.2Sr, 0.6Sr) during heat-treatment and extrusion were investigated. As-cast sample 0Sr contains typical long period stacking ordered (LPSO) phases and Mg_3RE. With Sr addition, amounts of LPSO phases decrease and are gradually replaced by the $Mg_{17}Sr_2$ phases. After homogenization and annealing treatment, profuse strip LPSO phases readily precipitate in grain interiors of sample 0Sr, while only $Mg_{17}Sr_2$ and Mg_3RE phases are detected in samples 0.2Sr and 0.6Sr. It suggests that the Sr addition would inhibit LPSO phases. After extrusion, the bimodal grain structures, the bulk and strip LPSO phases are detected in sample 0Sr, which can contribute to providing strengthening and extra strain hardening. In as-extruded sample 0.2Sr, finer recrystallized grain size, bulk $Mg_{17}Sr_2$ and LPSO phases (micron-scale) and Mg_5RE phase (nano-scale) are found due to the pre-annealing treatment. However, lower amounts of both nano-sized and macro-sized LPSO phases lead to the low ultimate strength (300 MPa). In sample 0.6Sr, the strip LPSO phases are readily formed even though the length and total amounts of LPSO phases decrease. More bulk $Mg_{17}Sr_2$ phases and LPSO phases are also precipitated, which lead to the more superior yield and ultimate strengths of 0.6Sr sample under higher temperature, as compared with the 0Sr sample.

Keywords: Mg alloys; LPSO; Sr; Bimodal grains; Mechanical property

1. Introduction

Magnesium alloys have great potential of reducing vehicle weight because of their high specific strength and stiffness [1-7]. In the past decade, the Mg-Gd-Y-Zn based alloys containing long period stacking ordered (LPSO) structures have been shown to exhibit excellent mechanical properties, including the high tensile strength of over 500 MPa at room temperature [8-12]. The outstanding property can be ascribed to the refinement of α-Mg matrix, precipitation of Mg-RE nano-particles, and formation of both strip LPSO phases within grain interiors and bulk LPSO phases along grain boundaries [11, 12]. The strip LPSO phases with inter-distances of nano-meter scale can readily improve yield strength of Mg alloys via second phase strengthening mechanism of impeding dislocations movement in α-Mg matrix [3, 13, 14]. Besides that, effect of the bulk LPSO phase (micron-scale) on strength of Mg alloy has also been given particular attention [15, 16]. In fact, basal slip is the dominant deformation mode in bulk LPSO phase at room temperature [17-19]. The Schmid factor for basal slipping is extremely low under tension along extrusion direction (ED), since most of basal planes in LPSO phase are in parallel with ED in conventional as-extruded Mg alloys [17-21]. Accordingly, the elongated LPSO phases in as-extruded Mg alloys are able to enhance the strength via short-fiber reinforcing mechanism, because of their large particle length, high aspect ratio and directional distribution. In other words, both strip and bulk LPSO phases would be beneficial for strengthening the Mg alloys.

In this sense, efforts of promoting LPSO phase formations have been attempted, including varying the extrusion parameters of temperature, ratio and rate, and mechanical properties can be tailored to some extents [22-26]. Furthermore, micro-alloying with particular elements in the Mg-Gd-Y-Zn based alloys has also been shown as another effective way to optimize the LPSO phase morphology, quantity and distribution. For example, Wang et al. found the Ca addition can induce formation of LPSO in the as-cast Mg-2.5Zn-2.5Y-1Mn (at.%) alloy, and the mechanical properties are enhanced due to the more LPSO phases [27] . Li et al. attempted to add the Mn element in Mg-2.5Zn-2.5Y (at.%) alloy and observed the higher area fraction of LPSO phases with increasing the Mn content [28]. Recently, Zhang et al. reported that the new precipitations can be induced, and the morphology

and distributions of LPSO phases are also varied by incorporating Zr element in Mg-Gd-Zn alloys [29]. In particular, the Sr element is an effective grain refinement element in Mg alloy and can reduce the stacking fault energy of α-Mg matrix [30]. However, the effect of Sr alloying on LPSO phases formation and mechanical property of the Mg-Gd-Y-Zn based alloy has rarely been attempted. Moreover, the previously reported Mg-Gd-Y-Zn based alloys usually contain high content of Zn element, so another purpose of present work is to investigate tendency of the LPSO phase formation with reduced amount of Zn addition and also the possibility of substitution of Sr for Zn. In this study, second phases and mechanical properties of alloys with and without Sr addition, Mg-6Gd-3Y-0.1Zn-xSr (x=0, 0.2, 0.6) were studied to clarify above issues.

2. Experimental

The cast billets of Mg-Gd-Y-Zn alloys with different Sr additions are prepared by melting the commercial pure Mg, pure Zn, pure Sr, Mg-30Gd and Mg-30Y master alloys and pouring the melt into cylinder mould with mixture protection gas of SF_6 and CO_2 (1:100). The nominal composition of the samples is designed as Mg-6Gd-3Y-0.1Zn- xSr (x=0, 0.2, 0.6). Actual compositions of the as-cast billets are measured and are listed in Table 1 (named as samples 0Sr, 0.2Sr and 0.6Sr respectively). The as-cast samples are homogenized at high temperature of 540 ºC for 24 h. In following with that, the as-homogenized samples are annealed at 400 ºC for 2 h. Purpose of the annealing treatment is to induce the precipitations prior to extrusion, and promote the following dynamic recrystallization. The billets are also indirectly extruded into the rod at extrusion ratio of 18 and ram speed of 0.3 mm/s at 400 ºC. It is noted that the initial billet for extrusions are as-homogenized for samples 0Sr and 0.6Sr, while it is the as-annealed state for sample 0.2Sr. The extrusion details are displayed in Table 1. The tensile test of as-extruded rod was conducted on the Shimadzu AG-XPlus250KN at strain rates of 1×10^{-3}/s along the extrusion direction. Microstructures of the samples were examined by optical microscopy (OM, Olympus GX) and scanning electron microscope (SEM, JEOL JEM-2100F) with energy dispersive spectrometer (EDS). X-ray diffraction (XRD, Philips PW3040/60 X'Pert PRO with Cu K_α radiation) was used to characterize the macro-texture and second phases.

3. Results

Fig. 1 shows SEM images and EDS results of the as-cast samples, and the typical dendritic microstructures are observed. In the as-cast sample 0Sr, the second phases in both strip and granular shapes distribute along grain boundaries or between the dendritic arms. The strip phase, as indicated by the arrow in position 1#, has a composition of Mg96.02RE2.79Zn1.2 (at.%), while the granular phase in position 2# contains 8.11 at.% of RE, 1.51 at.% of Zn and the balanced Mg element. Combined with the XRD results in Fig. 2a, the strip and granular particles are determined as LPSO (i.e., $Mg_{12}REZn$) and Mg_3RE phases respectively, which are exactly the same as the previous reports [11, 12]. With 0.2 wt.% of Sr addition, eutectic phases in the as-cast sample B exhibit some changes in their compositions, and the Zn elements are partially substituted by Sr. For example, the strip (3# point) and granular phases (4# point) contain Mg94.35RE3.66(Zn, Sr)1.99 (at.%) and Mg92.34RE6.93(Zn, Sr)0.73 (at.%) respectively. The XRD results also demonstrate the co-existence of $Mg_{12}REZn$ and Mg_3RE phases in sample 0.2Sr, so the particles in 3# and 4# points are identified LPSO and Mg_3RE phases accordingly. With further addition of 0.6 wt.% Sr, however, the strip phase disappears, while some bulk phases with compositions of 4.48 at.% Sr, 2.38 at.% RE and balanced Mg are detected, as shown in Fig.1c. The atomic percentage of Sr is apparently larger than that of RE, so the bulk phase can be identified as $Mg_{17}Sr_2$ accordingly to the Mg-RE-Sr ternary phase diagram [31]. Besides, the granular phase with atomic composition of Mg80.94RE18.04(Zn, Sr)0.53 (at.%) remains, and it can be classified as Mg_3RE phase, even though the Zn elements are partially substituted by Sr.

Fig. 3 demonstrates that the dendritic microstructures of as-cast samples disappear after the high temperature homogenization treatment. The second phases in the sample 0Sr almost dissolve into α-Mg matrix, while amount of the remained phases in samples 0.2Sr and 0.6Sr increases with the increased addition of Sr element. The un-dissolved phases evolve to be spherical and are determined to be Mg_3RE phases according to the XRD results in Fig. 2. Moreover, some network shaped $Mg_{17}Sr_2$ phases are also detected in as-homogenized sample 0.6Sr, as verified by XRD patterns. The optical images in Fig. 3 displays that average grain sizes of the as-homogenized sample 0Sr, 0.2Sr and 0.6Sr evolve to be ~175 μm~ 378 μm and

~480 μm respectively. After the following annealing treatment, a high density of second phases precipitates both in grain interiors and along grain boundaries (Fig. 4). The as-annealed samples display distinct microstructure features. For example, in sample 0Sr, numerous long-rod-shape phases and dotty phases are found to distribute in grain interiors, as indicated by the arrows in position 1# and 2# in Fig. 4b, and the compositions correspond to Mg96.26RE2.31Zn1.43 (at.%) and Mg91.1RE8.9 (at.%) respectively. According to the composition, morphology and XRD results, the rod and dotty phases should be LPSO and Mg_3RE phases. In sample 0.2Sr, on the other hand, the LPSO phases disappear, and the network second phases distribute along grain boundaries, with EDS composition of 3.81 at.% RE, 3.19 at.% Sr, 0.38 at.% Zn and balanced Mg (position 3# in Fig. 4d). The network phase is similar to the bulk contrast in as-cast sample 0.6Sr, which corresponds to the $Mg_{17}Sr_2$ phase. Besides, the similar Mg_3RE phases are found in grain interiors according to the composition profile of position 4# in Fig. 4d. Formation of both $Mg_{17}Sr_2$ and Mg_3RE phase are also confirmed by XRD results (Fig. 2). In sample 0.6Sr, the discontinuous $Mg_{17}Sr_2$ phases are found to precipitate along grain boundaries due to the high Sr content of 8.14 at.% and low concentration of RE (position 5# in Fig. 4e). Moreover, the similar Mg_3RE phases are found in grain interiors in high density (position 6# in Fig. 4e, EDS result of Mg74.96RE25.04).

Fig. 5 displays the optical images and grain size distributions of as-extruded samples along longitudinal sections. It should be noted that the initial billets of as-extruded sample 0Sr and 0.6Sr are in the as-homogenized states, while both homogenization and pre-annealing treatments are conducted on the initial billet of sample 0.2Sr. The as-extruded sample 0Sr exhibits a bimodal grain size feature, with both dynamically recrystallized (DRXed) grains and un-DRXed grains, as indicated by arrows. Volume fraction of the DRXed grains regions corresponds to ~ 70%, and average size of the DRXed grains is sharply refined to be ~ 5 μm. The un-DRXed grains are deformed into streamline shape along the extrusion direction. The as-extruded sample 0.2Sr exhibits a higher volume fraction of DRXed grains (~ 82%), compared with that of the sample 0Sr. The pre-existing second phases due to

pre-annealing should play the critical role, which would be discussed in the following section. Average grain size of the as-extruded 0.2Sr alloy is as fine as that of sample 0Sr, ~ 4.5 μm. For as-extruded sample 0.6Sr, even higher fraction of DRXed grains is produced, ~ 90%, and it can be ascribed to higher amount of micron-scale second phases (indicated by arrows in Fig. 4f). However, the average size of DRXed grain increases to some extent, ~ 8.7 μm.

The recrystallization behaviors can be further confirmed by macro-texture. It has been reported that DRXed grains usually exhibit RE-texture in the RE-containing Mg alloy, i.e., c-axis rotating some angles away from radial direction (RD) of as-extruded bar [16, 32-34]. The un-DRXed grain, on the other hand, keeps the typical fiber feature of c-axis being parallel with RD [32]. Fig. 6 displays the typical (0001) texture of present as-extruded samples. In this sense, both the DRXed and un-DRXed textures can be detected in sample 0Sr, and it agrees well with the optical images of Fig. 5a and also the previous reports. In sample 0.2Sr and 0.6Sr, however, only DRXed texture can be found, which should be due to the apparently decreased fraction of un-DRXed grains region.

In order to clarify the mechanism of grain growth due to the second phase formations, SEM images of as-extruded samples in both low and high magnifications are displayed in Fig. 7. The observation is conducted on cross-section of bar. In the 0Sr sample, micron-scale phases in irregular shape are sharply elongated and should be dynamically formed by precipitation during hot deformation (Fig. 7a), as compared with that of as-homogenized sample (Fig. 3a). Fig. 7b shows that the micron-sized bulk phase exhibits the typical morphology feature of LPSO. Besides, profuse nano-scale rod-like second phases are also observed in grain interiors with inter-distance of ~100 nm, as indicated by the arrows. XRD results (Fig. 2) demonstrate that the LPSO phase is dominated in as-extruded sample 0Sr. Fig. 8 directly proves that the LPSO phases are formed in as-extruded 0Sr sample. Thus, both the bulk phase and rod-like phase are determined as LPSO phase. In as-extruded sample 0.2Sr, however, both LPSO phase in dark contrast and $Mg_{17}Sr_2$ phases in bright contrast appear and distribute along ED (Fig. 7c). The bulk LPSO phases are

substituted by $Mg_{17}Sr_2$ phases, as compared with sample 0Sr. Moreover, numerous nano-phases in plate-shape are detected in grain interiors, and distribute in particular angles with each other (Fig. 7d). The plate phases are similar to previously reported Mg_5RE phase [11, 12], which is also confirmed by present EDS results. Thus, the bulk LPSO/$Mg_{17}Sr_2$ phases, both in the micron size, and plate Mg_5RE phases in nano-scale are found to precipitate in as-extruded sample 0.2Sr. In sample 0.6Sr, higher amounts of bulk $Mg_{17}Sr_2$ phases are formed after hot extrusion, and some granular LPSO phases distribute among them (Fig. 7e). The nano-scale LPSO phases in reduced length compared with that of sample 0Sr are also found (Fig. 7f). In other word, the Sr addition can suppress the bulk LPSO phase formations, and high amount of RE element would dissolve into the bulk $Mg_{17}Sr_2$ phases in both as-cast and as-extruded samples. Accordingly, amount of the nano-sized LPSO phase decreases due to the lower RE content remained in α-Mg matrix.

Finally, mechanical properties of the as-extruded samples at both room temperature (RT) and higher temperatures are displayed in Fig. 9. Under room temperature (Fig. 9a), the as-extruded sample 0Sr exhibits yield strength (YS) of 160 MPa, ultimate strength (UTS) of 352 MPa and elongation (EL) of ~14%. For sample 0.2Sr with pre-annealing treatment, however, YS of 165 MPa, UTS of 300 MPa and EL of ~9% are obtained. Both the UTS and EL decrease as compared with that of sample 0Sr. With more addition of 0.6 wt.% Sr, YS of the sample 0.6Sr can be increased to be ~260 MPa, and both UTS and EL can reach 340 MPa and 10% respectively. Under higher temperature, evolutions of YS and UTS with testing temperatures are displayed in Fig. 9b-d. The YSs of both 0Sr and 0.6Sr samples increase first, reaching the peak values of 256 MPa and 282 MPa at 180 ºC, and then decrease with temperature (Fig. 9c). The UTSs, on the other hand, decrease monotonically with temperature. Moreover, UTS of the 0Sr decreases quickly and becomes lower than that of 0.6Sr at 150 ºC. That is, the 0.6Sr sample exhibits more superior strength under higher temperature, as compared with the 0Sr sample.

4. Discussion

4.1 Microstructure evolution

The sample 0Sr exhibits the typical non-equilibrium solidification microstructure in the as-cast state, and the Zn addition of only 0.1 wt.% induces the LPSO phase formation, besides the other phases of Mg_3RE. With Sr addition of ~ 0.2 wt.%, however, volume fraction of the LPSO phases decreases according to the SEM observation. With further addition of 0.6 wt.% Sr, the LPSO phases in as-cast sample 0.6Sr disappear and are replaced by the Sr containing $Mg_{17}Sr_2$ phase. It suggests that the Sr addition suppresses the LPSO phase formation in the as-cast Mg-Gd-Y-Zn alloys. Despite of that, it is noted that high amount of RE element is also detected within the formed $Mg_{17}Sr_2$ phase, and the remained RE content within α-Mg matrix decreases consequently. During homogenization, most of the second phases dissolve and evolve to be the sphere shape. After the following annealing treatment, the as-annealed samples exhibit different microstructure features. Profuse strip LPSO phases readily precipitate among grain interiors in sample 0Sr, as previously reported [11, 12]. With small addition of 0.2 wt.% Sr, no obvious strip LPSO phases are found in the as-annealed sample 0.2Sr. However, the net-work shaped $Mg_{17}Sr_2$ phases appear along grain boundaries and Mg_3RE phases are formed in grain interiors. In as-annealed sample 0.6Sr, more $Mg_{17}Sr_2$ and Mg_3RE phases are detected. The above results show that the Sr addition would also inhibit the LPSO phase formations in the as-annealed Mg-Gd-Y-Zn samples.

During the following extrusion, both the bulk LPSO phases and strip LPSO phases dynamically precipitate along grain boundaries and interiors. The bulk LPSO phase would promote the DRX by particle stimulated nucleation (PSN) mechanism [16, 32]. However, the numerous strip LPSO phases with inter-distance of ~ 100 nm would restrict DRX by dragging the grain boundaries migrations. Consequently, the bimodal grain structures containing both DRX and un-DRXed grains are formed in the sample 0Sr. For as-annealed sample 0.2Sr, however, large amounts of $Mg_{17}Sr_2$ phases with RE dissolved are precipitated prior to the extrusion. Content of the RE element remained within α-Mg matrix decreases, and amount of the bulk LPSO phase dynamically formed during extrusion decreases. Moreover, the Sr addition would

inhibit the strip LPSO phase formation, as illustrated above. So the LPSO phases are not formed within grain interiors, while the Mg_5RE phases are precipitated, as shown in Fig. 7b. Both the pre-formed $Mg_{17}Sr_2$ and Mg_5RE phases are reported to enhance the DRX [12], so a higher degree of recrystallization occurs in as-extruded sample 0.2Sr and the macro-texture also proves the result. For as-homogenization sample 0.6Sr, on the other hand, the strip LPSO phases are readily formed in spite of the higher amount of Sr addition. However, both the length and total amounts of LPSO phases decrease, as compared with that of as-extruded sample 0Sr. Moreover, limited amount of granular LPSO phase distributes along ED. More $Mg_{17}Sr_2$ phases in macron size are precipitated due to the high content of Sr addition in Mg-RE-Zn based samples. The large amount of macron-scale phases would stimulate DRX via PSN mechanism, so the recrystallization is almost completed in sample 0.6Sr.

4.2 Mechanical properties

The as-extruded sample 0Sr is composed of three typical microstructure regions, including the refined DRXed grains with RE texture, the hot-worked un-DRXed region with fiber texture and the plate-like LPSO phase along the extrusion direction. The bimodal grain structure would contribute to the excellent combination of strength and ductility, i.e., the high UTS of 352 MPa and high elongation of ~14% (Fig. 9a). The average size of the DRXed grains can be effectively refined to be ~ 5 μm, which should lead to gain refinement hardening due to the high value of slope of Hall-Petch relation for Mg alloys [35]. In addition, the fine recrystallized grains exhibit unusual RE texture with much weaker intensity, as shown in Fig. 6. The randomization of basal texture would contribute to the increment of ductility, since more deformation modes of basal slips and twinning can be activated [36, 37]. The bimodal grain size would allow some easy slips in fine-grained regions, but delay slipping in the coarse-grained regions to the higher stress level. The massive activation of slips in fine DRXed grains can lead to macroscopic yielding due to the higher volume fraction [19]. The un-DRXed grains, on the other hand, can contribute to abundant work hardening ability, which leads to the high elongation of sample 0Sr (Fig. 9a). In fact, the fine or ultra-fine grains have limited capability of storing dislocations, while the

coarse grains are effective in dislocation accumulation [38]. Thus, the bimodal grain size can further accommodate newly formed dislocations until a much higher tensile strain. Moreover, it is reported that the incompatibility of deformation between fine and coarse grains can also result in the higher ductility, since strain partitioning and back stress can be induced and maintain a moderate work hardening [38].

Besides that, the nano-sized LPSO phases within grain interiors can lead to considerable strengthening due to the high density and limited inter-distances (~ 100 nm). The macro-sized LPSO along grain boundaries can also contribute to strengthening via fiber reinforcement mechanism. Since the length of LPSO phase is high enough (~60 μm), the aligned LPSO phase would act as a strong reinforcing component in Mg/LPSO extruded alloy, which has been confirmed in previous work by Hagihara [15].

With 0.2 wt.% of Sr addition, the as-extruded sample 0.2Sr contains finer DRXed grains, and volume fraction of DRXed grains increases by comparing with that of sample 0Sr, leading to the much lower average grain size. So the YS should have been increased due to the grain refinement hardening. However, the actual YS remains to be ~ 160 MPa, which is similar to that of sample 0Sr (Fig. 9a). It can be ascribed to the lower amount of both nano-sized and macro-sized LPSO phases. As discussed above, the pre-annealing treatment leads to the lower content of RE dissolved in the initial α-Mg matrix, which suppresses the nano-sized LPSO phase formations during hot extrusion. The as-extruded sample 0.2Sr contains only the Mg_5RE phase in length of ~ 1 μm and inter-distances of 1~3μm, so the strengthening effect is largely compromised. The lower content of macro-sized LPSO phases would also decrease the yield strength, as compared with that of sample 0Sr. Moreover, the extra strain hardening effect due to the bimodal grain size structure diminishes to some extents in sample 0.2Sr, since the higher volume fractions of DRX occurs, as seen in the optical images (Fig. 5) and macro-texture (Fig. 6). As a consequence, the elongation of as-extruded sample 0.2Sr decreases to be only ~ 9%, and the UTS evolves to be 300 MPa, which is lower than that of sample 0Sr (Fig. 9a).

With more addition of 0.6 wt.% Sr, on the other hand, the as-extruded sample

0.6Sr exhibits a YS of ~260 MPa, which is much higher than that of sample 0Sr (Fig. 9a). The high YS can be ascribed to formation of the both nano-scale LPSO phases and the micron-scale $Mg_{17}Sr_2$ and LPSO phases. As shown in Fig. 7, the as-extruded sample 0.6Sr regains profuse nano-scale LPSO phases within grain interiors, and the inter-distance is as low as ~ 90 nm. So the strip LPSO phases would increase the YS via second phase strengthening mechanism. Moreover, a higher volume fraction of macron-scale phases distributes along grain boundaries, which can act as an effective reinforcement in Mg based composite and enhance the YS via load transferring [18]. Even though the DRX is almost completed and the average grain size increases to be ~ 8.7 μm, the second phases compensate the strengthening lose and increase the YS. Moreover, the macron phases can also enhance UTS of the Mg alloys, since the macron phases usually keep elastic in the yielding point and would only fracture until a high tensile strain is reached [19]. Thus, the high UTS of 340 MPa is produced in as-extruded sample 0.6Sr.

Under higher temperature, on the other hand, the YSs of both 0Sr and 0.6Sr samples increase first with temperature (Fig. 9c). The precipitations due to the keep heating for 30 min under tensile testing should be the reason, which leads to obvious higher YS via second phase hardening. With continuing temperature increase, the YSs decrease gradually due to the lower deformation resistance under high temperature. The UTSs decrease monotonically with temperature (Fig. 9c). The decreased defect accumulations, i.e. decreased strain hardening ability, due to the recovery and recrysllization effect could be on reason. The high temperature softening of both matrix and hardening phases (in both nano and micron scales) should be another reason. It is noted that the 0.6Sr sample exhibits more superior strength under higher temperature, as compared with the 0Sr sample. The higher amounts of micron-scale $Mg_{17}Sr_2$ and LPSO phases should play the critical role in maintaining the high thermal resistance.

5. Conclusions

In summary, microstructures and mechanical properties of alloys with and

without Sr addition, Mg-6Gd-3Y-0.1Zn-xSr (x=0, 0.2, 0.6), were investigated. The as-cast sample 0Sr contains typical LPSO phases and Mg_3RE. With Sr addition, the LPSO phases in as-cast sample 0.6Sr disappear and are replaced by the Sr containing $Mg_{17}Sr_2$ phase. After homogenization and the annealing treatment, it is found the profuse strip LPSO phases readily precipitate in sample 0Sr, while only $Mg_{17}Sr_2$ and Mg_3RE phases are detected in samples 0.2Sr and 0.6Sr. It suggests that the Sr addition would inhibit the LPSO phase formations in the both as-cast and as-annealed Mg-Gd-Y-Zn samples.

After extrusion, the bimodal grain structures, the bulk and strip LPSO phases are detected in sample 0Sr, which can contribute to provide strengthening and extra strain hardening. In as-extruded sample 0.2Sr, however, finer DRXed grain size, $Mg_{17}Sr_2$ and LPSO phases (micron-scale) and Mg_5RE phase (nano-scale) are found due to the pre-annealing treatment prior to extrusion. The lower amounts of both nano-sized and macro-sized LPSO phases lead to the low UTS (300 MPa) and elongation (9%). In sample 0.6Sr, the strip LPSO phases are readily formed even though the length and total amounts of LPSO phases decrease. More micron-scale $Mg_{17}Sr_2$ phases and some bulk LPSO phase are also precipitated, which lead to the higher YS of 260 MPa and UTS of 340 MPa due to the load transferring mechanism. The higher amounts of micron-scale phases also contribute to the more superior strengths of 0.6Sr sample under higher temperature, as compared with the 0Sr sample.

Acknowledgement

The authors acknowledge the financial support from The Ministry of Education "Chunhui Plan" Cooperative Research Project (16201417), the Key Research Project of Xihua University (Z1520102), Xihua University Key Laboratory Open Fund Project (SZJJ2014-061), Scientific Research Project in Sichuan Province Department of Education (15201444) and National Natural Science Foundation of China (51601154).

References

[1] B. Song, R. Xin, G. Chen, X. Zhang, Q. Liu, Scripta Materialia, 66 (2012) 1061-1064.

[2] H. Pan, Y. Ren, H. Fu, H. Zhao, L. Wang, X. Meng, G. Qin, Journal of Alloys and Compounds, 663 (2016) 321-331.

[3] H. Pan, G. Qin, M. Xu, H. Fu, Y. Ren, F. Pan, Z. Gao, C. Zhao, Q. Yang, J. She, B. Song, Materials & Design, 83 (2015) 736-744.

[4] A.A. Luo, Journal of Magnesium and Alloys, 1 (2013) 2-22.

[5] G. Bi, Y. Li, S. Zang, J. Zhang, Y. Ma, Y. Hao, Journal of Magnesium and Alloys, 2 (2014) 64-71.

[6] H. Pan, G. Qin, Y. Ren, L. Wang, S. Sun, X. Meng, Journal of Alloys and Compounds, 630 (2015) 272-276.

[7] Q. Huang, A. Tang, S. Ma, H. Pan, B. Song, Z. Gao, M. Rashad, F. Pan, Journal of Materials Engineering and Performance, 25 (2016) 2356-2363.

[8] M. Kiani, I. Gandikota, M. Rais-Rohani, K. Motoyama, Journal of Magnesium and Alloys, 2 (2014) 99-108.

[9] T. Li, K. Zhang, X. Li, Z. Du, Y. Li, M. Ma, G. Shi, Journal of Magnesium and Alloys, 1 (2013) 47-53.

[10] B. Lv, J. Peng, Y. Peng, A. Tang, Journal of Magnesium and Alloys, 1 (2013) 94-100.

[11] Z. Yu, Y. Huang, W. Gan, C.L. Mendis, Z. Zhong, H.G. Brokmeier, N. Hort, J. Meng, Materials Science and Engineering: A, 657 (2016) 259-268.

[12] Z. Yu, Y. Huang, C.L. Mendis, N. Hort, J. Meng, Materials Science and Engineering: A, 624 (2015) 23-31.

[13] B. Song, N. Guo, R. Xin, H. Pan, C. Guo, Materials Science and Engineering: A, 650 (2016) 300-304.

[14] H. Pan, H. Fu, B. Song, Y. Ren, C. Zhao, G. Qin, Philosophical Magazine Letters, (2016) 1-7.

[15] K. Hagihara, A. Kinoshita, Y. Sugino, M. Yamasaki, Y. Kawamura, H. Yasuda, Y. Umakoshi, Acta Materialia, 58 (2010) 6282-6293.

[16] M. Yamasaki, K. Hashimoto, K. Hagihara, Y. Kawamura, Acta Materialia, 59 (2011) 3646-3658.

[17] M. Tane, Y. Nagai, H. Kimizuka, K. Hagihara, Y. Kawamura, Acta Materialia, 61 (2013) 6338-6351.

[18] K. Hagihara, N. Yokotani, Y. Umakoshi, Intermetallics, 18 (2010) 267-276.

[19] G. Garces, D.G. Morris, M. Muñoz-Morris, P. Pérez, D. Tolnai, C. Mendis, A. Stark, H. Lim, S. Kim, N. Shell, Acta materialia, 94 (2015) 78-86.

[20] Q. Huang, H. Pan, A. Tang, Y. Ren, B. Song, G. Qin, M. Zhang, F. Pan, Materials Science and Engineering: A, 664 (2016) 43-48.

[21] H. Pan, G. Qin, Y. Huang, Q. Yang, Y. Ren, B. Song, L. Chai, Z. Zhao, Journal of Alloys and Compounds, 688 (2016) 149-152.

[22] Y. Li, G.-z. Zhu, D. Qiu, D. Yin, Y. Rong, M.-X. Zhang, Journal of Alloys and Compounds, 660 (2016) 252-257.

[23] Z. Leng, J. Zhang, J. Sun, H. Shi, S. Liu, L. Zhang, M. Zhang, R. Wu, Materials & Design, 56 (2014) 495-499.

[24] Z. Leng, J. Zhang, C. Cui, J. Sun, S. Liu, R. Wu, M. Zhang, Materials & Design, 51 (2013) 561-566.

[25] L. Zhang, J. Zhang, Z. Leng, S. Liu, Q. Yang, R. Wu, M. Zhang, Materials & Design, 54 (2014) 256-263.

[26] C. Xu, J. Zhang, S. Liu, Y. Jing, Y. Jiao, L. Xu, L. Zhang, F. Jiang, M. Zhang, R. Wu, Materials & Design, 79 (2015) 53-59.

[27] J. Wang, J. Zhang, X. Zong, C. Xu, Z. You, K. Nie, Materials Science and Engineering: A, 648 (2015) 37-40.

[28] D. Li, J. Zhang, Z. Que, C. Xu, X. Niu, Materials Letters, 109 (2013) 46-50.

[29] J.S. Zhang, W.B. Zhang, X.Q. Ruan, L.P. Bian, W.L. Cheng, H.X. Wang, C.X. Xu, Materials Science and Engineering: A, 560 (2013) 847-850.

[30] J. Zhang, Y. Dou, G. Liu, Z. Guo, Computational Materials Science, 79 (2013) 564-569.

[31] X. Zhang, X. He, Y. Xue, Z. Wang, Q. Wang, Materials Technology, 29 (2014) 179-187.

[32] K. Oh-Ishi, C. Mendis, T. Homma, S. Kamado, T. Ohkubo, K. Hono, Acta Materialia, 57 (2009) 5593-5604.

[33] I.-H. Jung, M. Sanjari, J. Kim, S. Yue, Scripta Materialia, 102 (2015) 1-6.

[34] R. Alizadeh, R. Mahmudi, A.H. Ngan, T.G. Langdon, Advanced Engineering Materials, 18 (2016) 1044-1049.

[35] W. Yuan, R.S. Mishra, Materials Science and Engineering: A, 558 (2012) 716-724.

[36] B. Song, N. Guo, T. Liu, Q. Yang, Materials & Design, 62 (2014) 352-360.

[37] Q. Yang, B. Jiang, J. He, B. Song, W. Liu, H. Dong, F. Pan, Materials Science and Engineering: A, 612 (2014) 187-191.

[38] X. Wu, M. Yang, F. Yuan, G. Wu, Y. Wei, X. Huang, Y. Zhu, Proceedings of the National Academy of Sciences, 112 (2015) 14501-14505.

Fig. 1. SEM images and EDS results of the as-cast samples (a) 0Sr, (b) 0.2Sr and (c) 0.6Sr.

Fig. 2. XRD patterns of the samples (a) 0Sr, (b) 0.2Sr and (c) 0.6Sr, in as-cast, as-homogenization and as-annealed and as-extruded states.

Fig. 3. SEM and OM images of the as-homogenized samples (a, b) 0Sr, (c, d) 0.2Sr and (e, f) 0.6Sr, (a, c, e) SEM images and (b, d, f) OM images.

Fig. 4. SEM and EDS results of the as-annealed samples (a, b) 0Sr, (c, d) 0.2Sr and (e, f) 0.6Sr, (a, c, e) low-magnification images and (b, d, f) high-magnification images with EDS results.

Fig. 5. Optical images and grain size distributions of the as-extruded samples (a, b) 0Sr, (c, d) 0.2Sr and (e, f) 0.6Sr, (a, c, e) low-magnification images and (b, d, f) high-magnification images.

Fig. 6. Macro-textures of the as-extruded samples (a) 0Sr, (b) 0.2Sr and (c) 0.6Sr.

Fig. 7. SEM images of the as-extruded samples (a, b) 0Sr, (c, d) 0.2Sr and (e, f) 0.6Sr along the longitudinal sections, (a, c, e) low-magnification images and (b, d, f) high-magnification images.

Fig. 8. TEM image of the LPSO phases formed in as-extruded 0Sr sample, with insert of diffraction patterns.

Fig. 9. Engineering tensile stress-strain curves of the (a) as-extruded samples 0Sr, 0.2Sr and 0.6Sr at room temperature, (b) sample 0Sr and (d) sample 0.6Sr at higher temperature. (c) The evolutions of YS and UTS with testing temperatures of room temperature, 150 ºC, 180 ºC, 220 ºC and 270 ºC.

Table 1 Nominal and actual composition of the Mg-6Gd-3Y-0.1Zn- xSr (x=0, 0.2, 0.6) samples, and also the extrusion details.

Samples	Actual Compositions (wt.%)				Extrusion paths
	Gd	Y	Zn	Sr	
Sample 0Sr (Mg-6Gd-3Y-0.1Zn alloy)	6.47	3.35	0.15	---	Homogenization + extrusion
Sample 0.2Sr (Mg-6Gd-3Y-0.1Zn-0.2Sr alloy)	5.72	2.88	0.12	0.19	Homogenization + pre-annealing + extrusion
Sample 0.6Sr (Mg-6Gd-3Y-0.1Zn-0.6Sr alloy)	5.83	2.75	0.11	0.60	Homogenization + extrusion

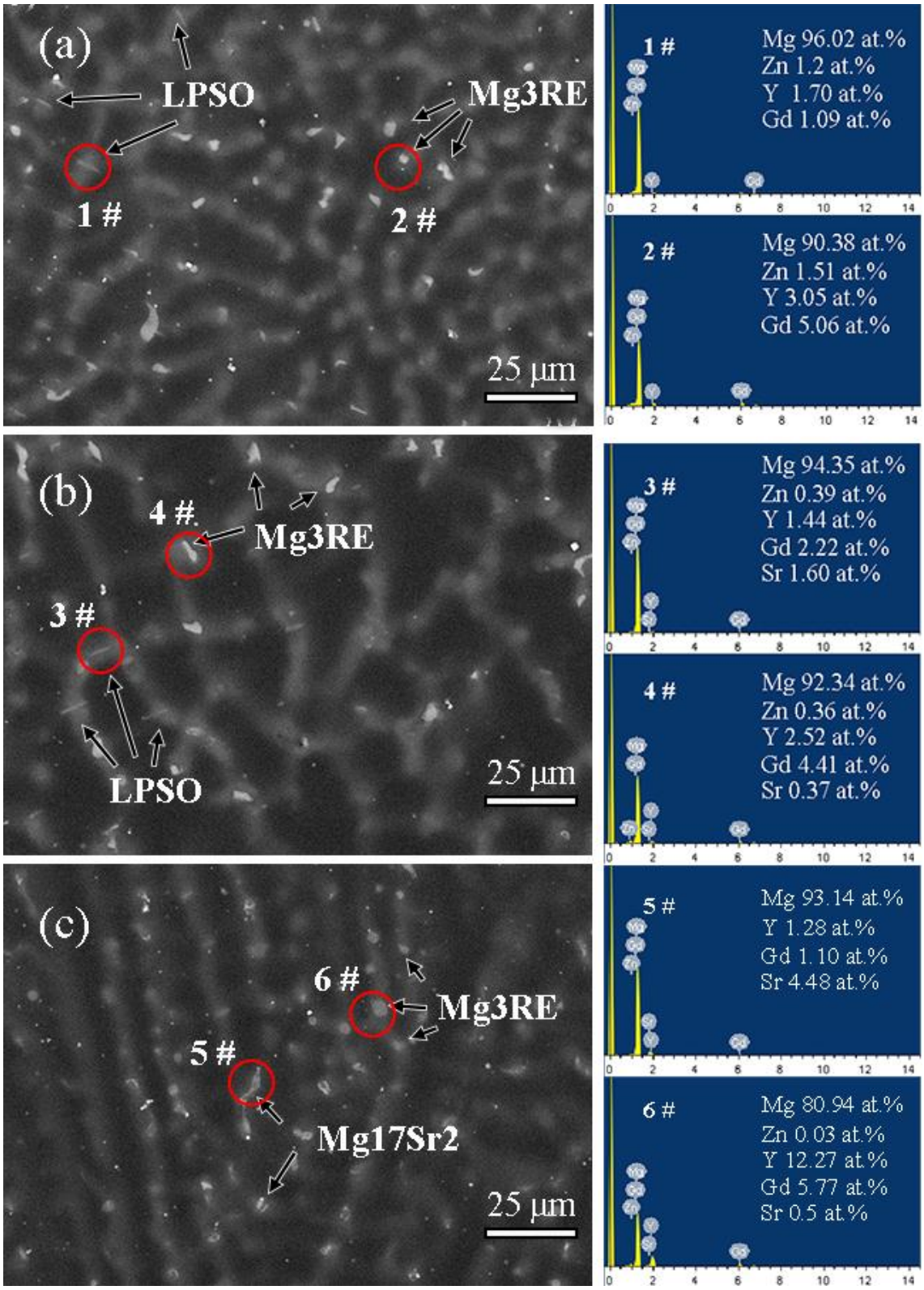

Fig. 1. SEM images and EDS results of the as-cast samples (a) 0Sr, (b) 0.2Sr and (c) 0.6Sr.

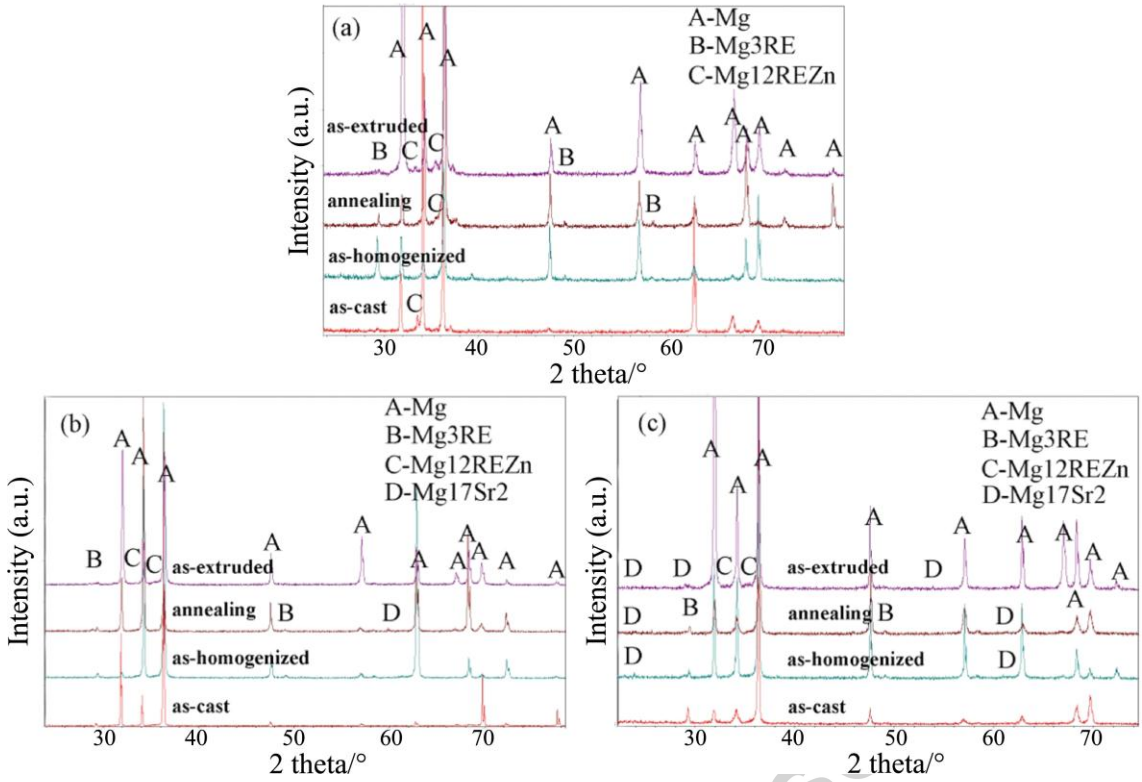

Fig. 2. XRD patterns of the samples (a) 0Sr, (b) 0.2Sr and (c) 0.6Sr, in as-cast, as-homogenization and as-annealed and as-extruded states.

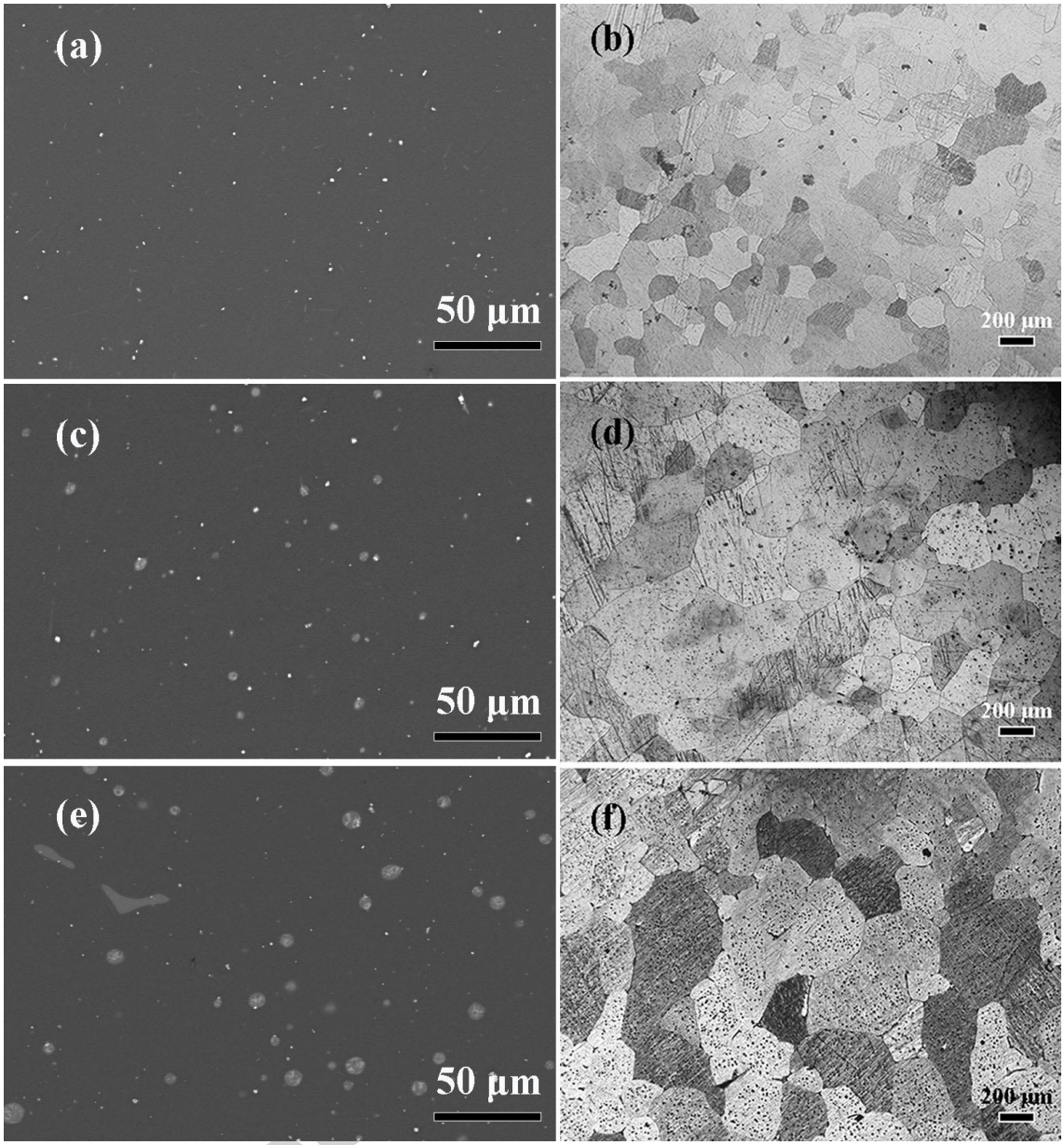

Fig. 3. SEM and OM images of the as-homogenized samples (a, b) 0Sr, (c, d) 0.2Sr and (e, f) 0.6Sr, (a, c, e) SEM images and (b, d, f) OM images.

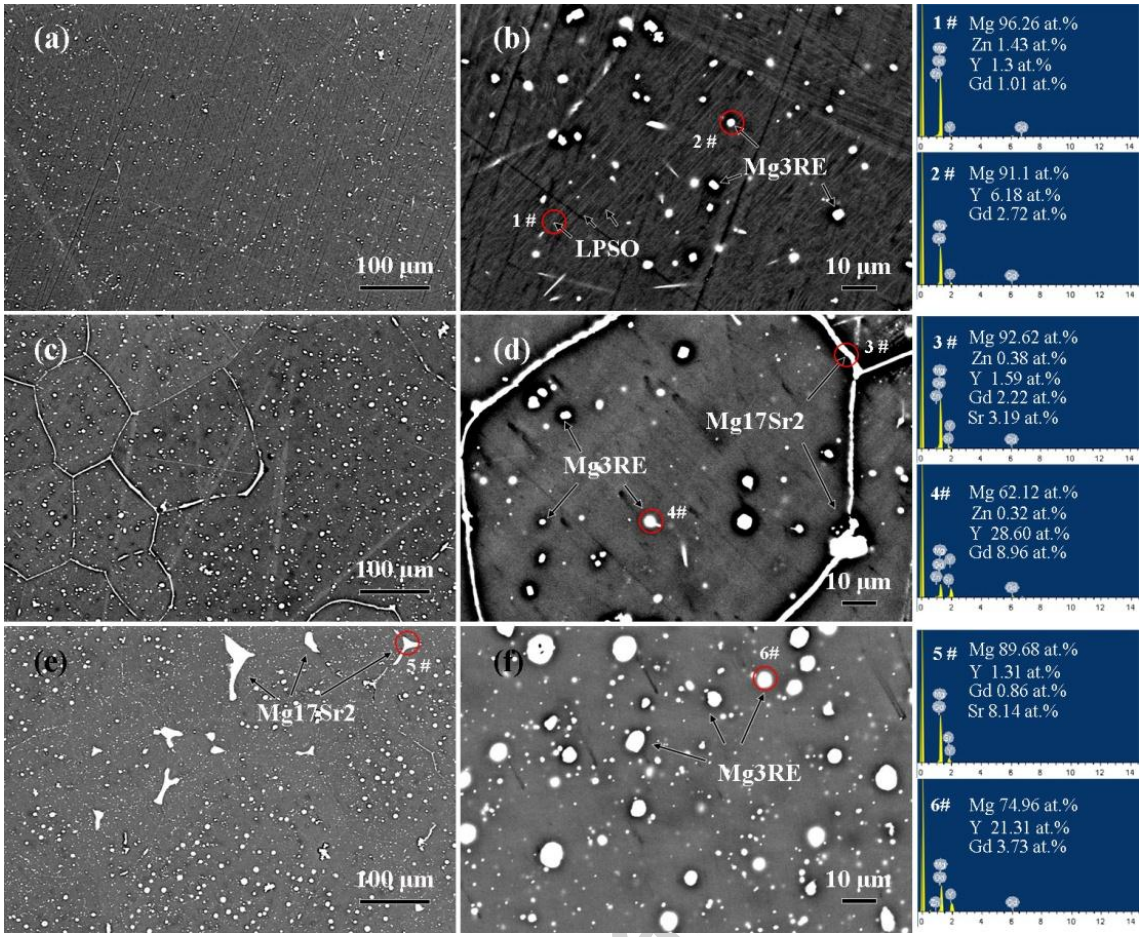

Fig. 4. SEM and EDS results of the as-annealed samples (a, b) 0Sr, (c, d) 0.2Sr and (e, f) 0.6Sr, (a, c, e) low-magnification images and (b, d, f) high-magnification images with EDS results.

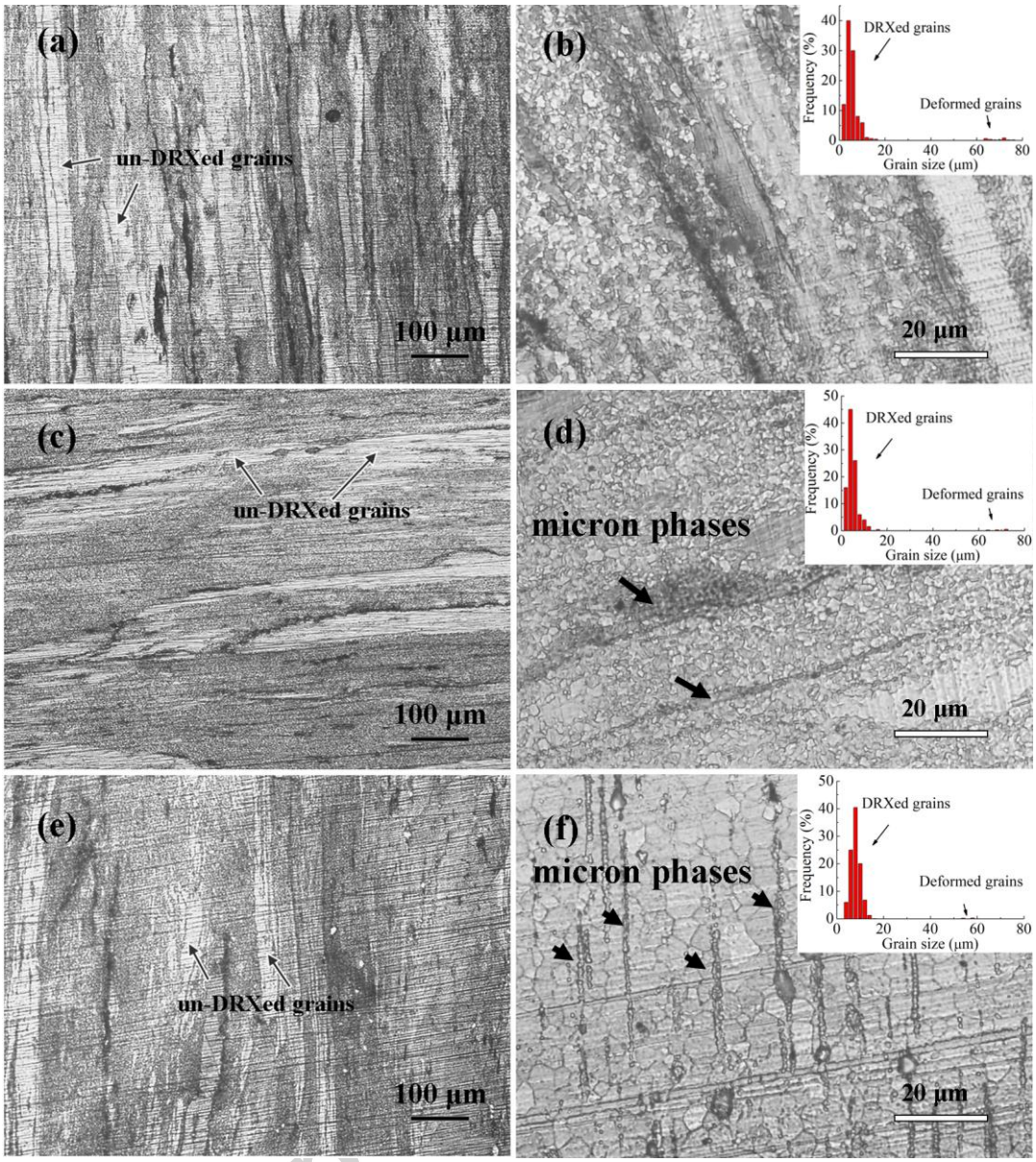

Fig. 5. Optical images and grain size distributions of the as-extruded samples (a, b) 0Sr, (c, d) 0.2Sr and (e, f) 0.6Sr, (a, c, e) low-magnification images and (b, d, f) high-magnification images.

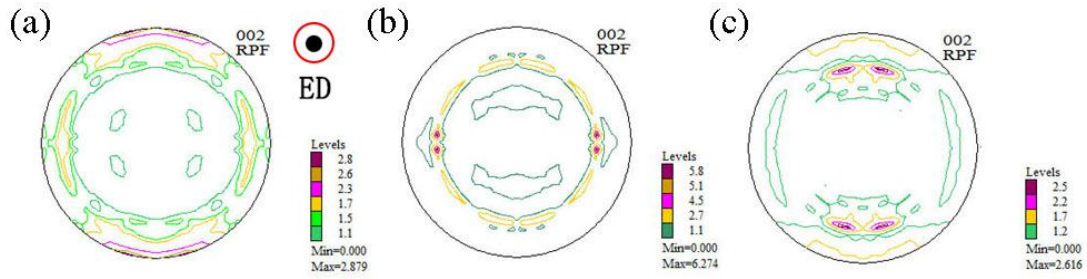

Fig. 6. Macro-textures of the as-extruded samples (a) 0Sr, (b) 0.2Sr and (c) 0.6Sr.

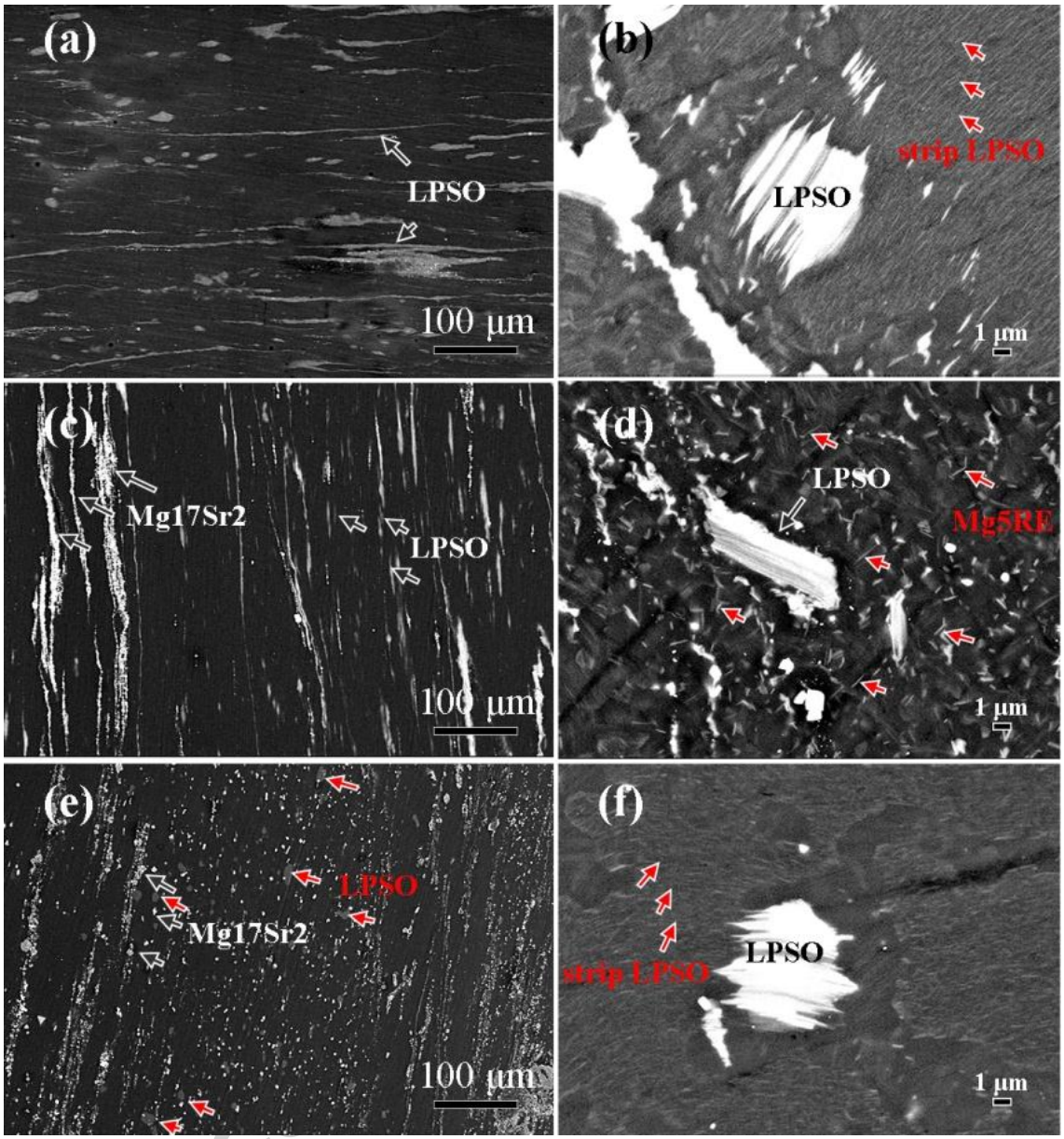

Fig. 7. SEM images of the as-extruded samples (a, b) 0Sr, (c, d) 0.2Sr and (e, f) 0.6Sr along the longitudinal sections, (a, c, e) low-magnification images and (b, d, f) high-magnification images.

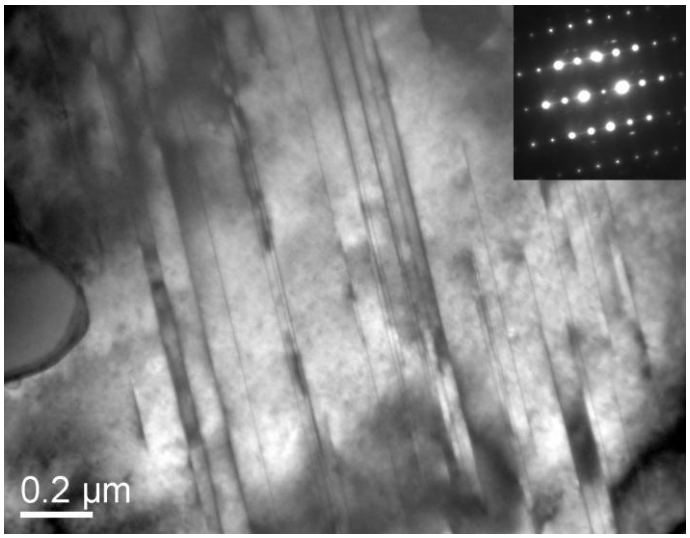

Fig. 8. TEM image of the LPSO phases formed in as-extruded 0Sr sample, with insert of diffraction patterns.

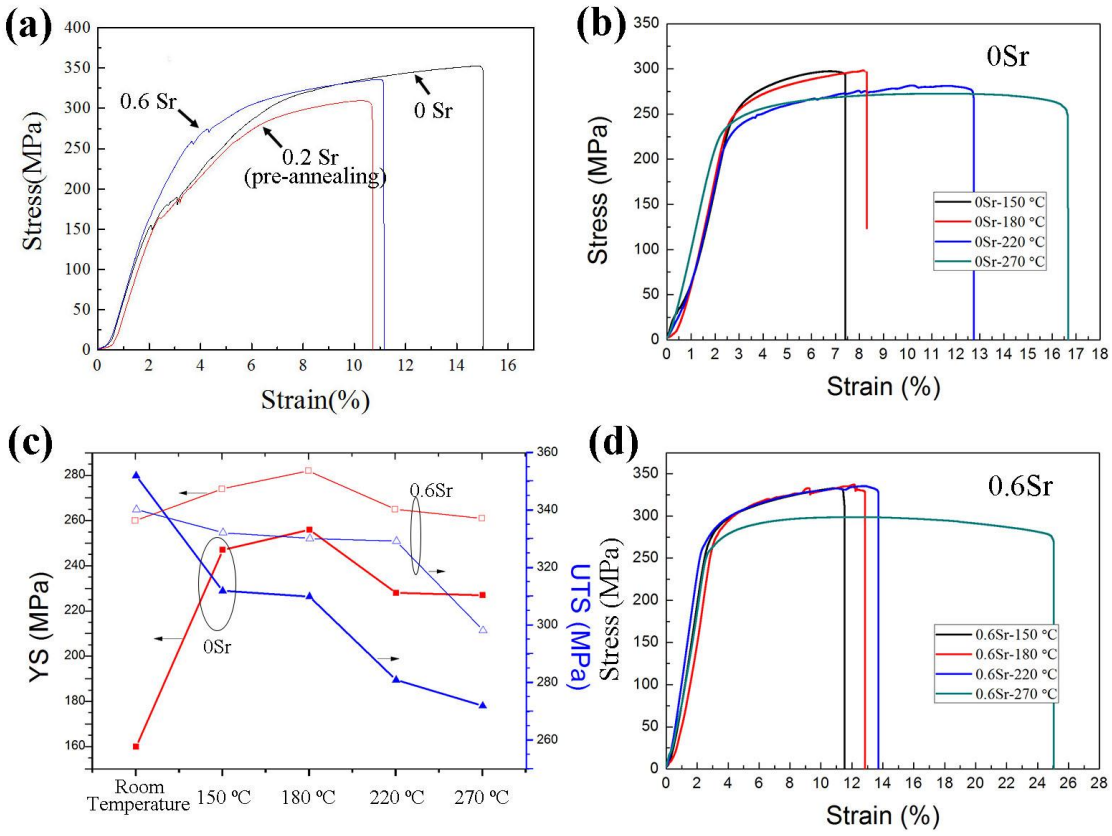

Fig. 9. Engineering tensile stress-strain curves of the (a) as-extruded samples 0Sr, 0.2Sr and 0.6Sr at room temperature, (b) sample 0Sr and (d) sample 0.6Sr at higher temperature. (c) The evolutions of YS and UTS with testing temperatures of room temperature, 150 ºC, 180 ºC, 220 ºC and 270 ºC.